

Review

Toward Direct Exploration of the Few-Femtosecond Dynamics of Electronic Coherence and Correlation in Quantum Materials Using Time- and Angle-Resolved Photoemission Spectroscopy

Kai Rosnagel^{1,2,3,†}  and Michael Bauer^{1,2,*,†} ¹ Institute of Experimental and Applied Physics, Kiel University, 24098 Kiel, Germany² Kiel Nano, Surface and Interface Science KiNSIS, Kiel University, 24118 Kiel, Germany³ Ruprecht Haensel Laboratory, Deutsches Elektronen-Synchrotron DESY, 22607 Hamburg, Germany

* Correspondence: bauer@physik.uni-kiel.de

† These authors contributed equally to this work.

Abstract: Over the last two decades, time- and angle-resolved photoemission spectroscopy (trARPES) has become a mature and established experimental technique for the study of ultrafast electronic and structural dynamics in materials. To date, most trARPES investigations have focused on the investigation of processes occurring on time scales of $\gtrsim 30$ fs, in particular, relaxation and thermalization, and have therefore been blind to the initial sub-10 fs dynamics related to electronic coherence and correlation effects. In this article, we illustrate how current trARPES setups reach their limits when it comes to addressing such extraordinarily short time scales and present an experimental configuration that provides the time, energy, and momentum resolutions required to monitor few-femtosecond dynamics on the relevant energy and momentum scales. We discuss the potential capabilities of such an experiment to study the electronic response of materials in the strong-field interaction regime at PHz frequencies and finally review a theoretical concept that may in the future even overcome the competing resolution limitations of trARPES experiments, as imposed by the time–bandwidth product of the probing laser pulse. Our roadmap for ultrafast trARPES indicates a path to break new experimental ground in quantum nonequilibrium electronic dynamics, from which new possibilities for ultrafast control of optical and electronic signals in quantum materials can be explored.

Keywords: electronic correlations; time-resolved photoemission; nonequilibrium phenomena; light–matter interaction



Citation: Rosnagel, K.; Bauer, M. Toward Direct Exploration of the Few-Femtosecond Dynamics of Electronic Coherence and Correlation in Quantum Materials Using Time- and Angle-Resolved Photoemission Spectroscopy. *Crystals* **2024**, *14*, 404. <https://doi.org/10.3390/cryst14050404>

Academic Editor: Claudio Cazorla

Received: 12 March 2024

Revised: 18 April 2024

Accepted: 18 April 2024

Published: 26 April 2024



Copyright: © 2024 by the authors. Licensee MDPI, Basel, Switzerland. This article is an open access article distributed under the terms and conditions of the Creative Commons Attribution (CC BY) license (<https://creativecommons.org/licenses/by/4.0/>).

1. Introduction

The time-domain study of photoinduced nonequilibrium phenomena in materials is a highly active and rapidly developing research field that contributes to our understanding of the properties of condensed matter in two important ways [1–3]: it provides valuable information about the correlations and dissipations that determine the equilibrium states of matter, but it also provides a novel means to create and explore short-lived transient as well as long-lived metastable nonequilibrium and quasi-equilibrium states that are inaccessible via conventional thermal pathways. By tracking the buildup and decay of the nonequilibrium state, such studies provide direct, real-time insights into the quasi-particle interactions between the involved charge, lattice, and spin degrees of freedom that take place on different characteristic time scales, as partially illustrated in Figure 1 (taken from [1]).

As the most direct probe of momentum-dependent changes in excited carrier populations and electronic band dispersions, trARPES offers an extraordinarily comprehensive view of the temporal evolution of the nonequilibrium charge degrees of freedom. For example, trARPES can monitor carrier–carrier and carrier–phonon interactions in real time,

information that is important for optimizing the electronic properties of materials for electronic devices. It can directly study nonequilibrium spin dynamics in magnetic materials on ultrafast time scales, which is central to the development of future ultrafast spintronic devices. In addition, trARPES studies of nonequilibrium dynamics in correlated materials such as high-temperature superconductors or charge-density waves (CDWs) can provide fundamental insights into the driving interactions of these fascinating phenomena, which can contribute to the development of corresponding materials for use in ambient conditions. As a final example, the technique allows the identification of metastable nonequilibrium states of matter and the characterization of their electronic structure, a topic of particular interest for the realization of novel and ultrafast optoelectronic devices. In recent years, several comprehensive review articles have been published on the technique of trARPES and its numerous applications, to which reference is made here instead of a detailed introduction [4–7]. Under the assumption of an instantaneous removal of the photoelectron from the surface (*sudden approximation*), which is typically fulfilled for sufficiently high kinetic energies of the photoelectron, the photoemission signal traces the one-particle spectral function $A(\mathbf{k}, \omega)$ [8,9], weighted by the photoemission dipole matrix element and the Fermi–Dirac function, and their changes upon photoexcitation. Here, \mathbf{k} denotes the electron momentum and ω the electron energy in the initial N -particle state. $A(\mathbf{k}, \omega)$ particularly accounts for energy renormalization and lifetime effects due to correlations and interactions in the many-body initial state of the system.

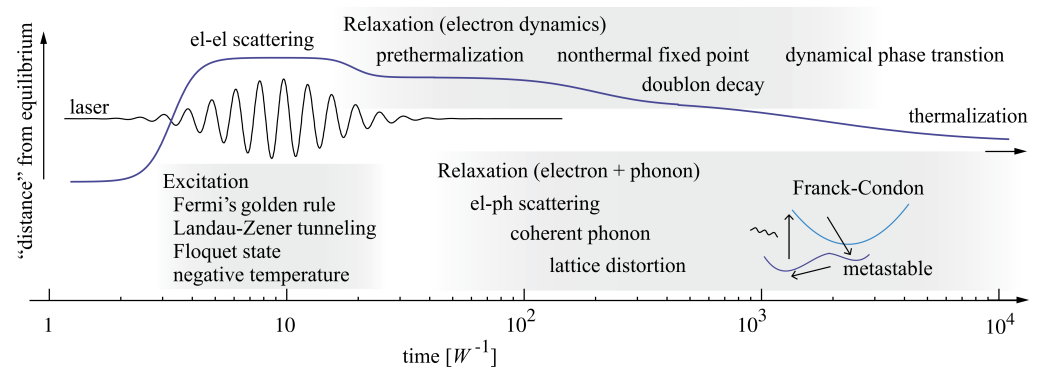


Figure 1. Schematic temporal evolution of a correlated electron material in a pump–probe experiment with different physical processes taking place on characteristic time scales. Time is shown in units of the intrinsic electronic time scale W^{-1} , where W is the (eV scale) electronic bandwidth. Reprinted from [1]. Copyright (2014) by The American Physical Society.

Figure 2 shows a schematic of a typical trARPES setup using extreme ultraviolet (XUV) pulses to probe the sample response in photoemission upon excitation with femtosecond near-infrared (NIR) pulses. Various types of setups have been realized in the recent past and a list of currently installed systems with their main specifications can be found in Ref. [4].

Many different topics have been addressed in numerous trARPES studies over the last decade. These include, for example, the investigation of carrier thermalization and the associated pathways in energy–momentum space [10–12], electron–phonon interactions [13,14], photoinduced phase transitions in charge-ordered correlated materials [15–17], energy-gap and quasiparticle dynamics in high-temperature superconductors [18,19], a transient Lifshitz transition of Fermi surface topology [20], field-driven carrier dynamics in topological insulators [21], ultrafast and valley-selective excitonic and free-carrier processes in bulk and single-layer semiconducting transition-metal dichalcogenides (TMDCs) [22–26], the formation of Floquet–Bloch states at the surface of a topological insulator [27], and spin and band dynamics associated with ultrafast demagnetization processes [28–30]. The time resolutions of these experiments, as usually specified by the full width at half maximum (FWHM) of the pump–probe cross-correlation signal, typically remain in the range of $\gtrsim 30$ fs (for a comprehensive overview of the specifications of trARPES instruments installed worldwide, see

again Ref. [4]). This limitation affects the time-domain access to the initial processes during and after photoexcitation, which are governed by electronic correlations and electronic decoherence, typically associated with ultrashort characteristic time scales in the range of a few femtoseconds, especially for strongly correlated materials with their relevant eV energy scales.

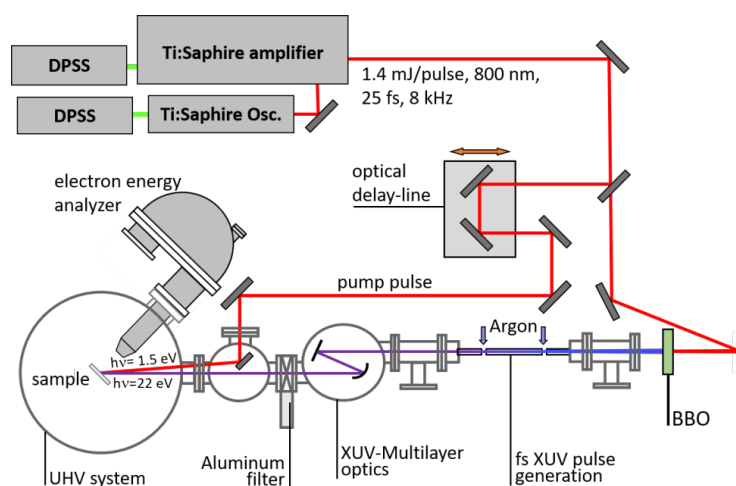


Figure 2. Schematic of an experimental setup for time- and angle-resolved photoemission. The NIR output of a low-repetition Ti:sapphire amplifier system is used for sample excitation (pump) as well as for the generation of XUV pulses in a high-harmonic process for time-delayed probing of the sample response via photoemission. The energy and momentum distributions of the photoemitted electrons are characterized using a hemispherical electron energy analyzer.

Some hints of the wealth of different phenomena that can occur in this time regime come from previous theoretical work. In a photoexcited Mott insulator, carrier relaxation due to electron–electron interaction can drive the system into a nonthermal state with a complicated electronic momentum distribution [31]. The authors suggested that such states might be observable in experiments on sufficiently short time scales where the electronic system is still decoupled from the surrounding thermal bath of phonons. Golež et al. investigated the effect of dynamical screening in photoexcited Mott insulators [32]. They reported a filling and reduction of the Mott gap due to the rapid change in the screening environment on characteristic inverse bandwidth time scales. In addition, a significant shortening of the doublon–hole recombination time was observed, caused by the interaction with the transient formation of low-energy screening modes. Another theoretical study of the pulsed, near-resonance excitation of a Mott-insulator state emphasized the interplay of coherent and incoherent processes in the formation of the final nonequilibrium state [33]. The authors observed that the initial dynamics was due to virtual Floquet states in the presence of the pump, followed by interaction-induced population of the upper Hubbard band from these states. Finally, Shen et al., simulating time-resolved photoemission data within a simplified model for a CDW insulator, observed a transient gap closure that lasted only slightly longer than the duration of the pump pulse [34]. The authors concluded that, on these ultrafast time scales, the electronic CDW order and the gap in the electronic energy spectrum decouple.

Experimentally resolving such processes and disentangling them from other interactions, and establishing a hierarchy of characteristic time scales of purely electronic interactions, requires experimental schemes that simultaneously provide spectral and temporal resolutions that match the relevant characteristic energy and time scales. Depending on the problem, the time resolution of the experiments should allow monitoring of purely electronic processes before coupling to other degrees of freedom occurs or before the electronic coherence in the system is lost.

2. Current Temporal Resolution Limits of trARPES: Few-Femtosecond Dynamics in Two Prominent Layered Quantum Materials

The current limitations of trARPES in entering the interesting few-femtosecond time domain are illustrated below based on results from previous studies of the ultrafast photoexcitation and electronic order dynamics in the layered CDW compounds $1T$ -TaS₂ and $1T$ -TiSe₂ [35–38]. For both compounds, the electronic structures [39–46] and ultrafast spectral responses [15,17,35–37,47] indicate the presence of significant electron correlation effects in addition to strong electron–phonon coupling.

2.1. Photoexcitation of a (Possible) Mott-Insulator Phase in $1T$ -TaS₂

$1T$ -TaS₂ exhibits a complex phase diagram that includes a high-temperature metallic phase, an incommensurate and a nearly commensurate CDW phase at intermediate temperatures, and, finally, below $T = 180$ K, a low-temperature commensurate CDW (CCDW) phase coexisting with a possible, much-discussed Mott-insulator phase [48–51]. Figure 3a shows a high-resolution ARPES intensity map of $1T$ -TaS₂ obtained with synchrotron radiation ($h\nu = 96$ eV) at $T = 33$ K, i.e., in the combined CCDW Mott-insulator phase. The CDW reconstruction of the electronic structure is most pronounced in the clear sub-band splittings along $\bar{\Gamma} - \bar{M}$, the strong band backfolding along $\bar{M} - \bar{K}$, and the large spectral gap opening at the edge of the original Brillouin zone (BZ) (midway between \bar{M} and \bar{K}). Here, we are interested in the possible Mott contribution to the phase. It is spectrally evidenced by a Mott–Hubbard-type gap near the $\bar{\Gamma}$ point at the Fermi level E_F , which separates the lower Hubbard band (LHB), representing singly occupied sites, and the upper Hubbard band (UHB), representing doubly occupied sites (doublons) (the UHB above E_F is not visible in Figure 3a because it is unoccupied in thermal equilibrium).

Before pump-pulse excitation, the gap is also clearly visible in trARPES data near $\bar{\Gamma}$ [left panel of Figure 3b], despite the limited energy resolution (400 meV) of the trARPES setup used in this study [35]. The right panel of Figure 3b shows trARPES data recorded 65 fs after photoexcitation of the sample with 30 fs NIR pump pulses at a fluence in the range of several mJcm^{-2} . The data clearly show a closing of the possible Mott–Hubbard gap upon excitation, implying the destruction of the Mott-insulator phase. The temporal evolution of the gap suppression can be followed from the photoemission intensity at E_F as a function of the pump–probe delay [Figure 3c]. The data show a quasi-instantaneous gap collapse within the duration of the pump pulse, with a time constant of less than 20 fs. The result agrees well with the results of a related trARPES study of $1T$ -TaS₂ which also reported the collapse of the Mott gap on time scales faster than the 30 fs resolution of the experiment [17].

The ultrafast response time is direct evidence for an electronic origin of the gap, strongly supporting the interpretation as a Mott–Hubbard gap. The measured upper limit of the time constant is consistent with an electronic hopping time $\tau_{\text{hop}} = \hbar/W \approx 1$ fs to 8 fs, which sets the time scale for the response of the correlated electron system to sudden changes [52,53] (where $W = 80$ meV to 400 meV corresponds to the width of the split-off Ta $5d$ band that straddles E_F [42]).

The exceptionally fast electronic response of the Mott–Hubbard gap spectral region of $1T$ -TaS₂ was also confirmed in a more recent trARPES study, which was performed at much lower pump fluences ($\approx 100 \mu\text{Jcm}^{-2}$) to avoid a suppression of the CCDW Mott insulating state [36]. Selected results of the study are shown in Figure 3d,e. Upon photoexcitation, the photoemission spectra show an instantaneous depopulation of the LHB and its repopulation on a few–100 fs time scale [see the green-colored photoemission intensity transient in Figure 3e]. On similar time scales, one can additionally observe the buildup and decay of an excitation continuum above E_F . The most interesting feature, however, is a distinct transient spectral peak above E_F , visible only at and near the temporal overlap of the pump and probe pulses. The authors interpret this feature as a spectroscopic signature for doublon formation, i.e., a transient population of the UHB across the Mott–Hubbard gap. Interestingly, the decay of the UHB population occurs on much faster time scales than

the spectrally overlapping excitation continuum [cf. corresponding photoemission intensity transients in Figure 3e], suggesting that the microscopic processes responsible for the decay of the excitation continuum and the doublon population are different. The authors conclude that the decay of the excitation continuum is due to electron–electron scattering, whereas the observed loss of the UHB must be explained by local electron–electron correlations. Analysis of the UHB photoemission intensity transient gave a value of 20 fs as an upper limit for the doublon recombination time, which in turn is compatible with the expected electronic hopping time. The experimental data also indicated an even faster thermalization of the excited carriers within the transiently populated UHB.

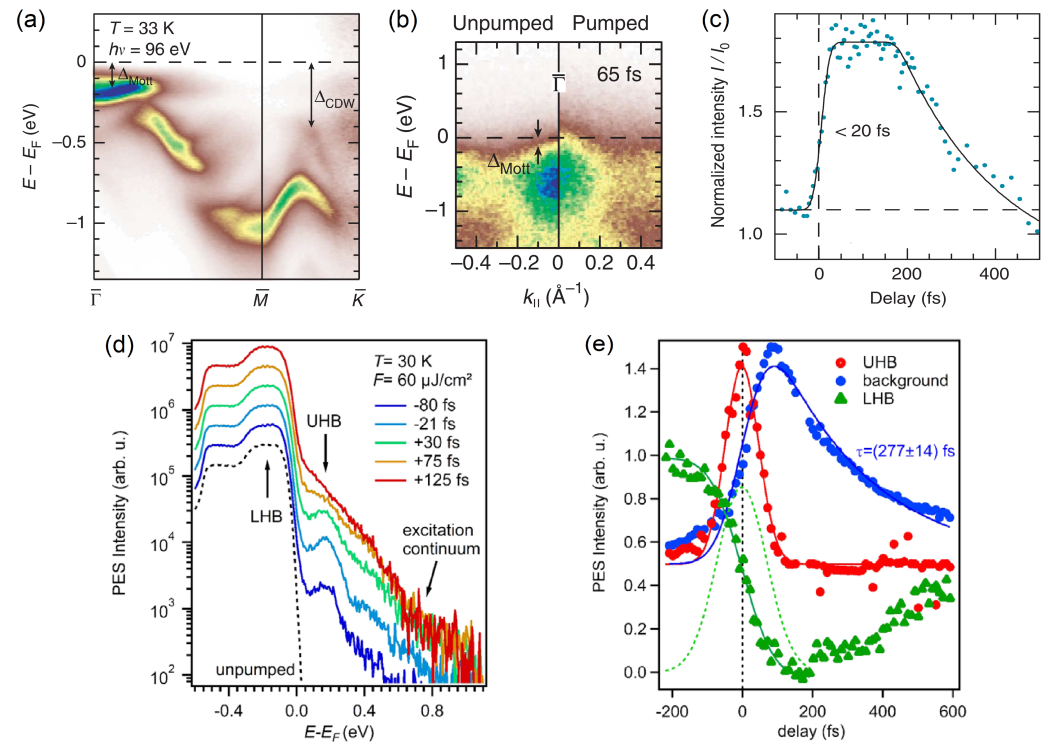


Figure 3. Ultrafast dynamics of the Mott-insulator phase in 1T-TaS₂. (a) Measured band dispersion along the $\bar{\Gamma} - \bar{M} - \bar{K}$ high-symmetry path for the commensurate CDW phase of 1T-TaS₂. Sample temperature and photon energy of the angle-resolved photoemission spectroscopy (ARPES) measurement are indicated. Photoemission intensity is represented in a false-color scale. The arrows mark the Mott–Hubbard gap Δ_{Mott} and the CDW gap Δ_{CDW} . (b) trARPES snapshots taken before optical pumping and at a pump–probe delay of 65 fs at the $\bar{\Gamma}$ point of 1T-TaS₂ (absorbed pump energy density: 300 Jcm^{-3} ; equilibrium sample temperature: 110 K). The arrows indicate the Mott–Hubbard gap. (c) Time dependence of the ARPES intensity at the $\bar{\Gamma}$ point. The energy interval over which the intensity has been integrated is $[-0.12, 0 \text{ eV}]$. (d) Transient photoemission spectra of 1T-TaS₂ obtained for an equilibrium sample temperature of 30 K and a pump fluence of $60 \mu\text{Jcm}^{-2}$. The curves are offset for better visibility. (e) Temporal evolution of the upper Hubbard band (UHB) spectral signature in direct comparison with the underlying continuum and electronic gap, as well as the lower Hubbard band (LHB) intensity loss. Solid lines are fits to the experimental data using appropriate fitting functions. The temporal derivative $-dI/dt$ of the least mean square fit of the LHB dynamics is shown as a dashed line for comparison with the UHB signal. Curves are rescaled for better visibility. (a) reprinted, (b,c) adapted from [35]. (d,e) reprinted from [36]. Copyright (2018) by the American Physical Society.

2.2. Ultrafast Suppression of a (Possible) Excitonic Insulator Phase in 1T-TiSe₂

The peculiarity of 1T-TiSe₂ that has attracted some interest in the past is a commensurate $(2 \times 2 \times 2)$ CDW occurring below a temperature of 200 K [54,55]. It has been proposed that the CDW state arises from an excitonic insulator instability [45,56,57], driven by purely

electronic interactions and accompanied by a periodic lattice distortion that is only an accidental byproduct [58].

Recently, time-domain experiments have been used to address this problem, as the observed characteristic time scales in the system response should provide information about the dominant driving interactions [35,37,38,59,60]. TrARPES snapshots from one of our studies of this compound are shown in Figure 4a [37]. The top panel shows a spectrum recorded before the arrival of the 30 fs pump pulse, reflecting the electronic structure of 1T-TiSe₂ in the CDW ground state. The spectral signature characteristic of the CDW phase is the downward dispersing (hole-like) band at \bar{M} , which is folded from $\bar{\Gamma}$ due to the formation of the $(2 \times 2 \times 2)$ CDW superlattice [43–45] (in the figure, $\bar{\Gamma}$ and \bar{M} indicate high-symmetry points of the BZ of the undistorted room-temperature phase). When the pump and probe pulses overlap in time (0 fs), an electron-like band appears, indicating the photoinduced population of excited states at and above E_F . The additional signal at $\bar{\Gamma}$, indicated by the dashed black line, is a replica of the hole-like band (solid black line) separated by the pump-photon energy of 1.5 eV due to laser-assisted photoemission (LAPE) [61]. At the same time, the spectral intensity of the hole-like band at \bar{M} is significantly reduced, before disappearing completely 30 fs after excitation [bottom panel in Figure 4a]. The latter observation suggests that the long-range CDW order in the electronic subsystem breaks down exceptionally quickly on sub-vibrational time scales below 30 fs, supporting an electronic origin of the CDW. In principle, an energy shift of the hole-like band towards E_F , indicating the closing of the CDW gap as the CDW order is lost [45], should also be visible in the data. However, the limited energy resolution of the trARPES experiment of ≈ 400 meV prevents the observation of this effect.

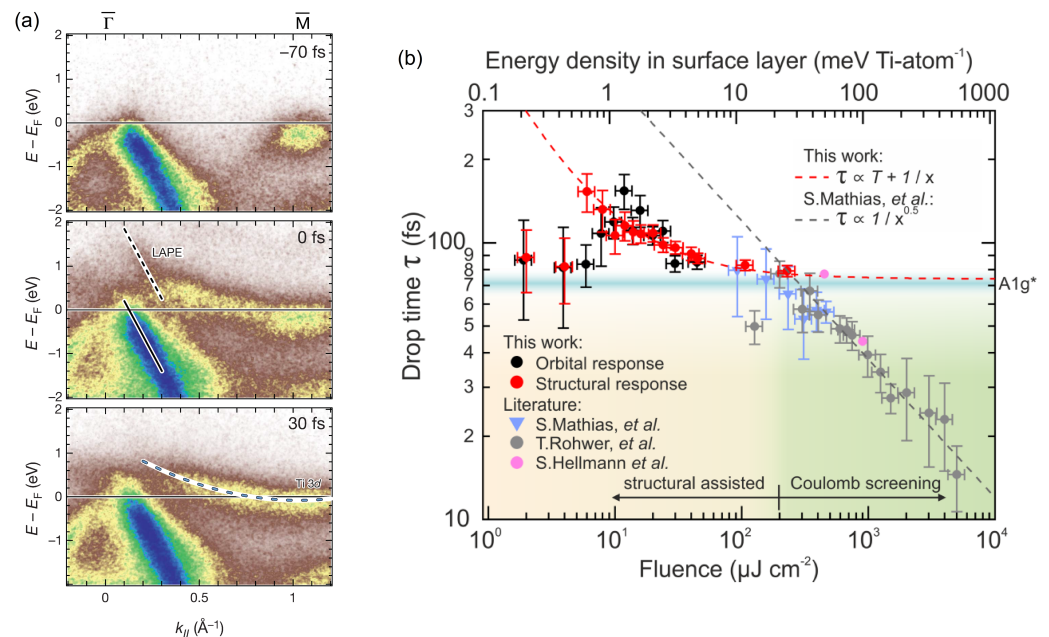


Figure 4. Ultrafast dynamics of the excitonic insulator phase in 1T-TiSe₂. (a) trARPES snapshots of 1T-TiSe₂ for increasing pump–probe time delays (pump–pulse fluence: 5 mJ cm^{-2}). The pump-induced spectral changes at \bar{M} indicate the suppression of the charge-ordered state. (b) Comparison of characteristic signal drop times indicating the suppression of a combined charge- and lattice-ordered state, compiled from different works [35,37,38,59]. In the high-fluence regime ($>200 \mu\text{J cm}^{-2}$), hot-carrier (Coulomb) screening is sufficiently fast to dominate the overall dynamics. (a) reprinted from [37]; (b) reprinted from [38].

The pump fluence dependence of the dynamics shows that CDW quenching accelerates with increasing excitation density. Figure 4b summarizes results on the photoinduced quenching dynamics from time-resolved X-ray diffraction [38] and trARPES

studies [35,37,59]. The characteristic fluence dependence indicates a complex interplay of structural and electronic degrees of freedom responsible for the stabilization of the low-temperature CDW-ordered phase in $1T$ -TiSe₂ [38]. Here, we focus on the high-fluence regime, where comparison with simulations suggests that hot-carrier (Coulomb) screening is important for perturbing order in the electronic subsystem. The characteristic buildup time for carrier screening in response to ultrashort laser excitation is the plasma oscillation period [62,63] which scales with $1/\sqrt{n}$, where n is the free-carrier density generated in the photoabsorption process. At the highest value of n , corresponding to the maximum excitation fluence of $\approx 5 \text{ mJcm}^{-2}$ applied in the experiment, the quench dynamics starts to enter the sub-20 fs time domain, beyond the time resolution of the experiment [37].

3. Pushing the Temporal Resolution Limit of trARPES: Entering the Sub-10 fs Time Regime

The above examples illustrate that ultrafast processes, which are mainly governed by electronic interactions or correlations, rely on time-domain experimental techniques with time resolutions of ≈ 10 fs and below. In this context, trARPES could uniquely provide an energy- and momentum-resolved view of the involved band-structure and carrier-population dynamics. However, this is only possible in a well-balanced experimental configuration, in which, in addition to the dynamical information, the relevant spectral information can be meaningfully resolved. The practical boundary conditions are defined by the characteristic time scales of carrier decoherence and the fundamental inter-relationship between the energy and time domains, as shown schematically in Figure 5a: access to the relevant energy scales associated with coherence times in the range of a few femtoseconds requires energy resolutions of a few 100 meV. From an experimental point of view, the ultimate limit is set by the time–bandwidth product of the probe pulse, which inversely links the time and energy resolution of time-domain spectroscopy.

Recently, our team succeeded in realizing a trARPES experiment that meets all the requirements and approaches the fundamental limit. The key measure to improve the time resolution of an existing system [64] was the implementation of a hollow-core fiber setup in the NIR pump line, which generates broadband light pulses that are then compressed to a few cycles (6.5 fs) [65]. The XUV probe line, based on high-harmonic generation, was not affected by this upgrade, so the energy resolution of the instrument remained the same. Details of the experimental setup are described in Ref. [66]. Figure 5b summarizes the experimental verification of the main specifications of the setup. The FWHM of the pump–probe photoemission cross-correlation signal measured at the sample position gives a value of 13 fs, well suited for resolving dynamics in the sub-10 fs regime. At the same time, an ultimate energy resolution of ≈ 200 meV could be confirmed (mainly limited by the time–bandwidth product of the 11 fs probe pulse).

In a first study of nonequilibrium carrier dynamics in graphite, we demonstrated the ability of the experiment to resolve and discriminate processes occurring on time scales below 10 fs [67]. The two plots in Figure 6a show energy distribution curves (EDCs) around E_F and at the H point of the BZ of graphite, recorded at different time delays after excitation with 6.5 fs pump pulses and compared to the measured equilibrium distribution at $T = 300$ K (black line). At the temporal overlap of pump and XUV probe pulse (0 fs), a clear spectral distortion is observed in the EDC, which evolves as a function of time [cf. right panel of Figure 6a]. This indicates the nascent nonthermal character of the carrier distribution on ultrashort time scales [12,68–71]. The quantitative analysis of the data allows disentangling the different processes involved in the buildup and decay of the nonthermal distribution on the relevant time scales from below 10 fs to several 10 fs [see Figure 6b]. In particular, it was possible to separate different stages during carrier thermalization dominated by either carrier–carrier or carrier–phonon interactions.

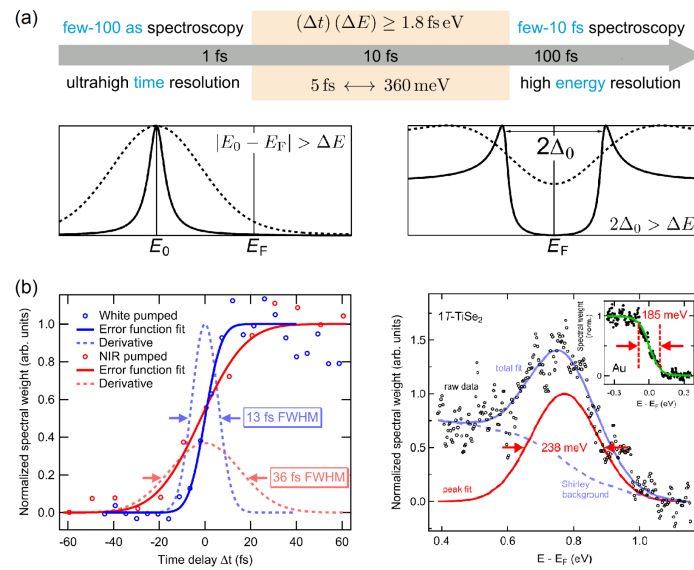


Figure 5. Few-femtosecond trARPES: requirements and realization. (a) Schematic representation of the different time regimes of ultrafast processes and the specific challenges with respect to temporal and/or spectral resolution. In the few-femtosecond time regime, spectral resolutions in the 100 meV range are required in order to still be able to resolve spectral peak shifts (bottom left) or gap closings (bottom right) on the characteristic energy scales. (b) Left: Comparison of NIR-pump/XUV-probe cross-correlation signals recorded with 11 fs probe pulses and 6.5 fs (blue) and 34 fs (red) pump pulses, respectively. The open dots show experimental photoemission transients from the transiently populated conduction band of 1T-TiSe₂. The solid lines are the results of fitting an error function to the experimental data. The dashed lines are the derivatives of the fit results, which are interpreted as approximations to the pump–probe cross-correlation curves. Right: EDC of 1T-TiSe₂ (open circles) recorded with 11 fs probe pulses ($h\nu = 22.1 \text{ eV}$) at $k_y = 0.3 \text{ \AA}^{-1}$ along the $\bar{\Gamma} - \bar{M}$ direction 40 fs after excitation with a 6.5 fs pump pulse. A Shirley background (dashed light blue line) was subtracted from the data before linewidth analysis. The red line is a Gaussian fit to the spectral peak in the experimental data, yielding a peak width of 238(10) meV (FWHM). Inset: EDC of polycrystalline Au (full circles) recorded with 11 fs probe pulses ($h\nu = 22.1 \text{ eV}$) at $T = 100 \text{ K}$. The green line is a fit of a Fermi–Dirac distribution function to the data and gives a width of 185(10) meV (12–88% width). For comparison, the time–bandwidth product gives a spectral width of the XUV pulse of 170 meV. (b) reprinted from [66], with the permission of AIP Publishing.

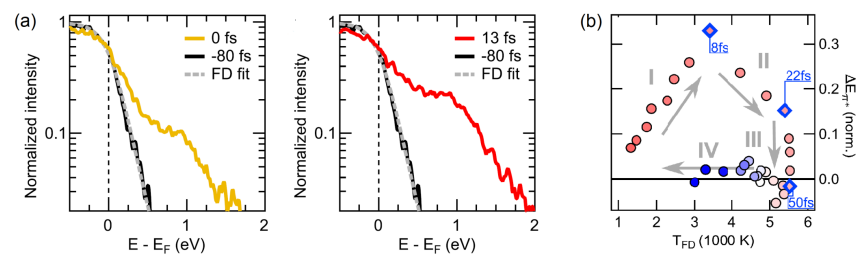


Figure 6. Few-femtosecond electron dynamics in graphite. (a) EDCs around E_F for pump–probe delays $\Delta t = 0 \text{ fs}$ and $\Delta t = 13 \text{ fs}$ derived from trARPES data near the Dirac cone in graphite compared to an EDC recorded before NIR excitation ($\Delta t = -80 \text{ fs}$). The dashed line is a fit of a Fermi–Dirac distribution function to the equilibrium EDC. (b) Different stages of thermalization of a photogenerated nonthermal hot electron distribution in graphite within the first 50 fs after time zero, as derived from a quantitative analysis of a complete series of trARPES snapshots. ΔE_{π^*} is a measure of the difference between the nonthermal and thermal electron distributions, T_{FD} is the apparent electron temperature derived from fitting a Fermi–Dirac distribution function to the EDC of the non-thermalized electron gas. (a,b) reprinted from [67]. Copyright (2018) by The American Physical Society.

A very similar trARPES experimental setup, which also achieves a time resolution in the 10 fs range (≈ 13 fs FWHM of the pump–probe cross-correlation), is described in Ref. [12]. In a study of primary thermalization events in graphene, the authors were able to distinguish between impact ionization and Auger recombination, processes that control the initial carrier relaxation in graphene in a time window up to ≈ 15 fs after photoexcitation. The measured energy resolution of the setup is worse compared to that reported in [66] (800 meV at optimum time resolution). To compensate for this limitation, the authors analyzed their data using a special momentum-to-energy conversion method. This takes advantage of the fact that, while energy resolution is intrinsically affected by the time–bandwidth product, the momentum resolution is unaffected. This method may also be applicable to other systems with similarly simple and well-known band dispersions, such as the linear dispersion of the Dirac cone in graphene.

The few-femtosecond trARPES results presented here represent a step toward the study of nonequilibrium electronic structure dynamics in the time domain of electronic coherences and correlations in materials. Together with other complementary time-resolved pump–probe techniques, this may in the future specifically contribute to further elucidate the exotic physical properties of quantum materials that arise from the quantum mechanical properties of their constituent electrons. This particularly includes attosecond to few-femtosecond time-resolved all-optical methods such as transient absorption spectroscopy in the visible [68,71], XUV [72,73], and soft X-ray spectral regime [74]. The exceptional (ultimately few-meV) energy resolution that can be achieved in principle by these techniques, and which is made possible by the independence of the time and frequency domains [75], can complement the unique momentum information of trARPES in such studies. In this context, the advances in the synthesis and investigation of novel low-dimensional and topological quantum materials provide an almost inexhaustible playground.

Finally, one may wonder about the role of photoemission-based attosecond streaking [76–78] or RABBIT (reconstruction of attosecond beating by interference of two-photon transitions) [79,80] in the study of electronic interactions in materials. So far, however, both experimental approaches could only be used to study the dynamics of the final states of photoemission but not to probe ultrafast changes in the electronic structure of the initial states. A major limitation, at least within a streaking experiment, is the limited energy resolution, which is in the range of several eV due to the attosecond time profile of the XUV pulses.

4. Future Perspectives of Few-Femtosecond trARPES: Exploring Quantum Interference and Overcoming the Time–Bandwidth Product

4.1. Few-Cycle Strong-Field ARPES at PHz Frequencies

Intense and few-cycle femtosecond pump pulses as part of a trARPES experiment provide unique opportunities for studying changes in the energy–momentum distribution of electronic states and their population due to interactions in the (nonperturbative) strong-field regime. The novel and exciting insights that can be gained from such studies were recently demonstrated in a trARPES experiment on field-driven Dirac currents at the surface of a topological material using THz pump pulses [21]. With a central excitation wavelength in the NIR and visible spectral range, it may become possible to similarly probe processes relevant to electric field-waveform control scenarios of optical and electronic properties in the PHz frequency range, i.e., on characteristic time scales of electronic decoherence in solids [81,82].

As an illustrative example, we propose a strong-field ARPES experiment on Rabi oscillations and Landau–Zehner–Stückelberg interferences in the excited state population in graphene, resulting from the interaction with few-cycle NIR pulses with a peak electric field strength E_0 in the Vnm^{-1} range. The study is motivated by recently performed photocurrent control experiments in graphene using the carrier–envelope phase (CEP) of few-cycle NIR laser pulses as a control parameter [83,84]. Numerical simulations showed that the detected net photocurrent observed for $E_0 \gtrsim 2 \text{ Vnm}^{-1}$ arises from suboptical-cycle

Landau–Zener–Stückelberg interferences, consisting of coherent repeated Landau–Zener transitions on the femtosecond time scale [see Figure 7a]. The characteristic signatures of the interferences can be seen in the energy–momentum distribution of the photoexcited carriers within the Dirac cone of graphene after passage of the excitation pulse [Figure 7b]. The black lines in Figure 7b indicate equienergy lines in resonance with multiples of the central photon energy. The quasi-periodic population patterns at the resonance energies are remnants of Rabi oscillations that occur in the transition regime between the (photon-driven) weak-field response and the (field-driven) strong-field response. The off-resonant populations, which show a clear asymmetry with respect to $k_x = 0$, are due to CEP-modulated Landau–Zener–Stückelberg interferences. The net photocurrent observed in [83] is a direct consequence of this asymmetry. Note that dissipative processes due to carrier–carrier scattering and carrier–phonon scattering were not considered in the simulations.

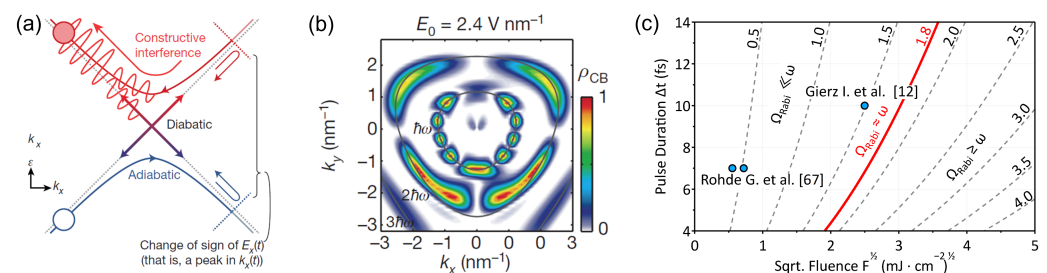


Figure 7. Few-femtosecond trARPES: entering the few-cycle strong-field regime. (a) Illustration of combined interband (Landau–Zener) and intraband transitions in the Dirac cone of graphene, which can act as a beam splitter for an electron wavefunction exposed to a light field in the strong-field regime. In a single oscillation of the electric field, the electron can experience the beam-splitting effect twice, resulting in two possible quantum paths to reach the conduction band. (b) Calculated residual conduction band population in graphene near the K point for different values of a peak electric field strength $E_0 = 2.4 \text{ V nm}^{-1}$ of the excitation laser pulse. The data show results for an 800 nm, 5.5 fs laser pulse with a carrier–envelope phase of $\pi/2$ and linear polarization along the x -direction. The plots show the population after the laser pulse has excited the sample and neglect dissipative processes due to interactions with electrons and phonons. Solid lines indicate the resonances, the energy difference between the valence and conduction bands corresponding to energies $h\nu$, $2h\nu$, and $3h\nu$ (from inside to outside), where $h\nu$ is the laser photon energy. Resonant populations indicate photon-driven processes, off-resonant populations indicate field-driven quantum path interference processes. (c) E_0 of few-cycle 800 nm laser pulses as a function of pulse duration and the square root of the incident pump fluence F . Constant values of E_0 in units of V nm^{-1} are marked by the gray dashed lines. The solid red line marks the boundary between the weak-field and the strong-field regime in graphene ($E_0 = 1.8 \text{ V nm}^{-1}$, $\gamma \approx 1$) reported in Ref. [83]. The blue circled points indicate the experimental laser pulse parameters used in trARPES experiments on graphite [67] and graphene [12]. (a,b) reprinted from [83], Springer Nature.

Few-femtosecond trARPES would be the ideal tool to map such energy–momentum distributions, which represent the microscopic picture behind the detected mesoscopic photocurrents: the characteristic momentum distribution patterns will only be visible on time scales shorter than the intrinsic dephasing and population relaxation times, which in graphene are of the order of a few femtoseconds (electron–electron scattering) up to several 10 fs (electron–phonon scattering) [12,67,69,85]. A limiting factor for the realization of this experiment can be space-charge effects due to pump pulse-induced multiphoton photoemission processes [86]. In the relevant pump fluence regime, space-charge effects can significantly distort the energy and momentum distribution of the electrons photoemitted by the probe pulse, ultimately preventing a meaningful evaluation of the recorded photoemission intensity maps.

Figure 7c displays the peak electric field strength E_0 of few-cycle 800 nm laser pulses as a function of pulse duration and the square root of the pump fluence F . The gray dashed

lines mark constant values of E_0 in units of Vnm^{-1} . The red line represents the formal boundary between the weak-field and the strong-field regime, corresponding to the Keldish parameter $\gamma = 1$ (expressed in the graph by the equality of the Rabi frequency Ω_{Rabi} and the angular frequency of the driving laser field ω). The three data points in the graph mark the experimental parameters used in two trARPES studies on graphite [67] and graphene [12]. The value of E_0 that the electrons experience inside the material was calculated assuming a refractive index of graphite of $n_{\text{Gr}} \approx 2.6$ [87,88] and, in the case of graphene, the refractive index of the underlying SiC substrate of $n_{\text{SiC}} \approx 2.6$ [83]. Both works focused on the time evolution of the energy distribution of the excited carriers but did not consider changes in the momentum distribution. The data still show that few-cycle NIR trARPES in the strong-field regime of interest are within reach. Such an experiment can provide valuable information not only on the energy–momentum dependence of quantum interference pathways but also on how the interferences are affected by decoherence due to dissipative interactions on electronic time scales. In the future, a successful implementation of such an experiment may stimulate further studies such as strong-field photoemission interferometry dealing with topological properties of two-dimensional materials [89], the reciprocal space exploration of coherently controlled electron trajectories [84], or energy- and momentum-resolved CEP-phase and two-pulse few-cycle control experiments in semiconducting monolayer TMDCs and derived heterostructures.

4.2. Coherent Multidimensional ARPES

We have argued above that for spectroscopic access to the regime of electronic time scales in materials it is necessary to realize a trARPES experiment that is balanced in terms of energy and time resolution. Nevertheless, one can wonder if it is possible to realize a trARPES experiment that simultaneously provides high energy resolution and high time resolution beyond the limits imposed by the time–bandwidth product.

A promising concept to achieve this goal is multidimensional spectroscopy, which has already been successfully applied in two-photon photoemission experiments on solids [90,91] and in the gas phase [92]. For example, these studies provided valuable insights into local coherences of plasmonic active nanostructures [90], surface and bulk state coherences at single-crystal surfaces [93,94], excitonic correlations in metals [95], and the dressing of electronic band structures of metals [91]. All these experiments were performed with photon energies in the NIR to near ultraviolet spectral range. XUV pulses would make it possible to apply this concept also to trARPES and thus considerably extend the accessible energy–momentum range. This would open up new possibilities to study electronic processes with simultaneously high time and energy resolution throughout the BZ (and beyond) or via transient spectral changes in (shallow) core-electron levels.

A recent theoretical work described and analyzed a possible experimental configuration that might be able to achieve this goal in the future [96]. The authors proposed to apply the concept of coherent multidimensional optical spectroscopy [97,98] to trARPES. Instead of following the response of the electronic structure to the optical stimulus with a single probe pulse, such types of experiments use two successive probe pulses locked in their relative phase. The additional information compared to conventional pump–probe experiments comes from the interference contribution to the detected probe signal. The effect on the transient photoemission signal is illustrated by the simulations from [96] shown in Figure 8. The authors consider a single occupied energy level that is suddenly shifted in energy. Figure 8a shows the calculated Wigner function N as a function of energy and time, which could be referred to as the time-dependent occupied density of states. The resulting time-resolved photoemission signal for a single Gaussian probe pulse and a phase-locked pair of probe pulses are shown in Figure 8b and c, respectively. Spectral details within the switching time window, which are completely missing in the single-probe experiment due to the limited spectral resolution, are well reproduced in the double-pulse experiment, demonstrating the superior information content of the multidimensional spectroscopy approach. The relative phase stabilization of a probe–pulse pair at a photon energy of

about 20 eV (a typical energy range used in common trARPES experiments [11,64,99–101]) requires a pulse-to-pulse timing stability in the range of 10 as, a value that can be achieved with actively stabilized delay stages [102].

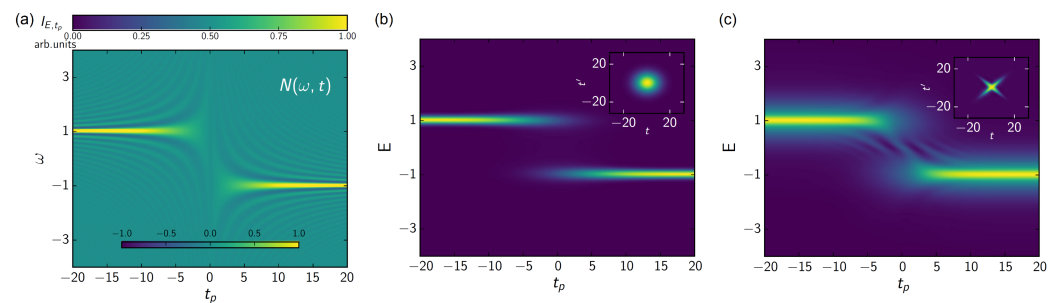


Figure 8. Two-dimensional spectroscopy applied to trARPES: illustration of the use of different probe pulse profiles in a time-resolved photoemission spectroscopy experiment. The system of interest is a single electronic level that is initially occupied and then suddenly energetically shifted at time $t_p = 0$. (a) Wigner transform $N(\omega, t)$ of the Green's function of the system. (b,c) Calculated momentum-integrated trARPES spectra obtained with different probe-pulse profiles [represented in the inset by the probe-pulse autocorrelation function $S(t, t')$], as a function of photoelectron energy and time. (b) Classical Gaussian probe pulse. The observed switching is resolution limited. (c) Nonseparable positive definite probe filter $S(t, t')$, which reproduces some of the features of the $N(\omega, t)$ in the photoemission spectrum due to its off-diagonal structure. (a–c) reprinted from [96]. Copyright (2017) by The American Physical Society.

5. Conclusions

In materials, the characteristic ≈ 1 eV energy scales of the electronic degrees of freedom lead to extremely fast dynamics of a few femtoseconds. In order to be able to observe the associated physical processes in detail at the fundamental level, real-time techniques are required that provide not only high time resolution, but also sufficient energy and momentum resolution. Few-femtosecond trARPES schemes, as described in this perspective, have these capabilities and can uniquely provide direct energy- and momentum-resolved information about the dynamics of electronic structures and quasiparticle populations on the characteristic time scales of electronic hopping and ultrafast light–matter interactions. Few-femtosecond trARPES can thus fill the time gap between few–100 as photoemission spectroscopy with ultrahigh time resolution and conventional few–10 fs trARPES with high energy resolution. This time gap is of great fundamental interest because it is here that electronic coherences and correlations arise and decay, and where nonthermal pathways, nonlinear responses, and dynamical interactions dominate. Entering this time regime with few-femtosecond trARPES will enable us to directly image the quantum electronic dynamics in materials in real time and to steer them toward novel nonequilibrium functionalities. Our vision is that we will be able to generate and probe coherent superpositions and correlated many-particle states, and manipulate these states on time scales comparable to or shorter than typical dephasing and interaction times.

Author Contributions: Writing—original draft preparation, K.R. and M.B.; writing—review and editing, K.R. and M.B. All authors have read and agreed to the published version of the manuscript.

Funding: This research was funded by the German Research Foundation (DFG) Project IDs 210740373, 389191527, and 465690255, and via the Collaborative Research Center (CRC) 925, Project ID 170620586 (Project B2).

Data Availability Statement: Not applicable.

Acknowledgments: We would like to thank Eduard Moos for creating Figure 7c of this publication.

Conflicts of Interest: The authors declare no conflicts of interest.

Abbreviations

The following abbreviations are used in this manuscript:

ARPES	angle-resolved photoemission spectroscopy
BZ	Brillouin zone
CCDW	commensurate charge-density wave
CDW	charge-density wave
CEP	carrier-envelope phase
EDC	energy distribution curve
FWHM	full width at half maximum
LAPE	laser-assisted photoemission
LHB	lower Hubbard band
NIR	near-infrared
RABBIT	reconstruction of attosecond beating by interference of two-photon transitions
TMDC	transition-metal dichalcogenide
trARPES	time- and angle-resolved photoemission spectroscopy
UHB	upper Hubbard band
XUV	extreme ultraviolet

References

1. Aoki, H.; Tsuji, N.; Eckstein, M.; Kollar, M.; Oka, T.; Werner, P. Nonequilibrium dynamical mean-field theory and its applications. *Rev. Mod. Phys.* **2014**, *86*, 779–837. [[CrossRef](#)]
2. Zhang, J.; Averitt, R.D. Dynamics and control in complex transition metal oxides. *Annu. Rev. Mater. Res.* **2014**, *44*, 19–43. [[CrossRef](#)]
3. De La Torre, A.; Kennes, D.M.; Claassen, M.; Gerber, S.; McIver, J.W.; Sentef, M.A. Colloquium: Nonthermal pathways to ultrafast control in quantum materials. *Rev. Mod. Phys.* **2021**, *93*, 41002. [[CrossRef](#)]
4. Gauthier, A.; Sobota, J.A.; Gauthier, N.; Xu, K.J.; Pfau, H.; Rotundu, C.R.; Shen, Z.X.; Kirchmann, P.S. Tuning time and energy resolution in time-resolved photoemission spectroscopy with nonlinear crystals. *J. Appl. Phys.* **2020**, *128*, 093101. [[CrossRef](#)]
5. Zhang, H.; Pincelli, T.; Jozwiak, C.; Kondo, T.; Ernstorfer, R.; Sato, T.; Zhou, S. Angle-resolved photoemission spectroscopy. *Nat. Rev. Methods Prim.* **2022**, *2*, 54. [[CrossRef](#)]
6. Na, M.X.; Mills, A.K.; Jones, D.J. Advancing time- and angle-resolved photoemission spectroscopy: The role of ultrafast laser development. *Phys. Rep.* **2023**, *1036*, 1–47. [[CrossRef](#)]
7. Boschini, F.; Zonno, M.; Damascelli, A. Time-resolved ARPES studies of quantum materials. *Rev. Mod. Phys.* **2024**, *96*, 015003. [[CrossRef](#)]
8. Damascelli, A.; Hussain, Z.; Shen, Z.X. Angle-resolved photoemission studies of the cuprate superconductors. *Rev. Mod. Phys.* **2003**, *75*, 473–541. [[CrossRef](#)]
9. Sobota, J.A.; He, Y.; Shen, Z.X. Angle-resolved photoemission studies of quantum materials. *Rev. Mod. Phys.* **2021**, *93*, 1–72. [[CrossRef](#)]
10. Schmitt, F.; Kirchmann, P.S.; Bovensiepen, U.; Moore, R.G.; Chu, J.H.; Lu, D.H.; Rettig, L.; Wolf, M.; Fisher, I.R.; Shen, Z.X. Ultrafast electron dynamics in the charge density wave material TbTe₃. *New J. Phys.* **2011**, *13*, 063022. [[CrossRef](#)]
11. Wallauer, R.; Reimann, J.; Armbrust, N.; Gdde, J.; Hfer, U. Intervalley scattering in MoS₂ imaged by two-photon photoemission with a high-harmonic probe. *Appl. Phys. Lett.* **2016**, *109*, 162102. [[CrossRef](#)]
12. Gierz, I.; Calegari, F.; Aeschlimann, S.; Chvez Cervantes, M.; Cacho, C.; Chapman, R.; Springate, E.; Link, S.; Starke, U.; Ast, C.; et al. Tracking Primary Thermalization Events in Graphene with Photoemission at Extreme Time Scales. *Phys. Rev. Lett.* **2015**, *115*, 086803. [[CrossRef](#)]
13. Gerber, S.; Yang, S.; Zhu, D.; Soifer, H.; Sobota, J.A.; Rebec, S.; Lee, J.J.; Jia, T.; Moritz, B.; Jia, C.; et al. Femtosecond electron-phonon lock-in by photoemission and X-ray free-electron laser. *Science* **2017**, *357*, 71–75. [[CrossRef](#)] [[PubMed](#)]
14. Hein, P.; Jauernik, S.; Erk, H.; Yang, L.; Qi, Y.; Sun, Y.; Felser, C.; Bauer, M. Mode-resolved reciprocal space mapping of electron-phonon interaction in the Weyl semimetal candidate Td-WTe₂. *Nat. Commun.* **2020**, *11*, 2613. [[CrossRef](#)]
15. Perfetti, L.; Loukakos, P.A.; Lisowski, M.; Bovensiepen, U.; Berger, H.; Biermann, S.; Cornaglia, P.S.; Georges, A.; Wolf, M. Time Evolution of the Electronic Structure of 1T-TaS₂ through the Insulator-Metal Transition. *Phys. Rev. Lett.* **2006**, *97*, 067402. [[CrossRef](#)] [[PubMed](#)]
16. Schmitt, F.; Kirchmann, P.S.; Bovensiepen, U.; Moore, R.G.; Rettig, L.; Krenz, M.; Chu, J.H.; Ru, N.; Perfetti, L.; Lu, D.H.; et al. Transient electronic structure and melting of a charge density wave in TbTe₃. *Science* **2008**, *321*, 1649–1652. [[CrossRef](#)]
17. Petersen, J.; Kaiser, S.; Dean, N.; Simoncig, A.; Liu, H.; Cavalieri, A.; Cacho, C.; Turcu, I.; Springate, E.; Frassetto, F.; et al. Clocking the Melting Transition of Charge and Lattice Order in 1T-TaS₂ with Ultrafast Extreme-Ultraviolet Angle-Resolved Photoemission Spectroscopy. *Phys. Rev. Lett.* **2011**, *107*, 177402. [[CrossRef](#)]

18. Smallwood, C.L.; Hinton, J.P.; Jozwiak, C.; Zhang, W.; Koralek, J.D.; Eisaki, H.; Lee, D.H.; Orenstein, J.; Lanzara, A. Tracking Cooper pairs in a cuprate superconductor by ultrafast angle-resolved photoemission. *Science* **2012**, *336*, 1137. [[CrossRef](#)] [[PubMed](#)]
19. Cortés, R.; Rettig, L.; Yoshida, Y.; Eisaki, H.; Wolf, M.; Bovensiepen, U. Momentum-Resolved Ultrafast Electron Dynamics in Superconducting $\text{Bi}_2\text{Sr}_2\text{CaCu}_2\text{O}_{8+\delta}$. *Phys. Rev. Lett.* **2011**, *107*, 097002. [[CrossRef](#)]
20. Beaulieu, S.; Dong, S.; Tancogne-Dejean, N.; Dendzik, M.; Pincelli, T.; Maklar, J.; Patrick Xian, R.; Sentef, M.A.; Wolf, M.; Rubio, A.; et al. Ultrafast dynamical Lifshitz transition. *Sci. Adv.* **2021**, *7*, eabd9275. [[CrossRef](#)]
21. Reimann, J.; Schlauderer, S.; Schmid, C.P.; Langer, F.; Baierl, S.; Kokh, K.A.; Tereshchenko, O.E.; Kimura, A.; Lange, C.; Gütde, J.; et al. Subcycle observation of lightwave-driven Dirac currents in a topological surface band. *Nature* **2018**, *562*, 396–400. [[CrossRef](#)] [[PubMed](#)]
22. Bertoni, R.; Nicholson, C.W.; Waldecker, L.; Hübener, H.; Monney, C.; De Giovannini, U.; Puppini, M.; Hoesch, M.; Springate, E.; Chapman, R.T.; et al. Generation and Evolution of Spin-, Valley-, and Layer-Polarized Excited Carriers in Inversion-Symmetric WS_2 . *Phys. Rev. Lett.* **2016**, *117*, 277201. [[CrossRef](#)] [[PubMed](#)]
23. Beyer, H.; Rohde, G.; Grubišić Čabo, A.; Stange, A.; Jacobsen, T.; Bignardi, L.; Lizzit, D.; Lacovig, P.; Sanders, C.; Lizzit, S.; et al. 80% Valley Polarization of Free Carriers in Singly Oriented Single-Layer WS_2 on Au(111). *Phys. Rev. Lett.* **2019**, *123*, 236802. [[CrossRef](#)] [[PubMed](#)]
24. Liu, F.; Ziffer, M.E.; Hansen, K.R.; Wang, J.; Zhu, X. Direct Determination of Band-Gap Renormalization in the Photoexcited Monolayer MoS_2 . *Phys. Rev. Lett.* **2019**, *122*, 246803. [[CrossRef](#)] [[PubMed](#)]
25. Karni, O.; Barré, E.; Pareek, V.; Georganas, J.D.; Man, M.K.; Sahoo, C.; Bacon, D.R.; Zhu, X.; Ribeiro, H.B.; O’Beirne, A.L.; et al. Structure of the moiré exciton captured by imaging its electron and hole. *Nature* **2022**, *603*, 247–252. [[CrossRef](#)] [[PubMed](#)]
26. Schmitt, D.; Bange, J.P.; Bennecke, W.; AlMutairi, A.A.; Meneghini, G.; Watanabe, K.; Taniguchi, T.; Steil, D.; Luke, D.R.; Weitz, R.T.; et al. Formation of moiré interlayer excitons in space and time. *Nature* **2022**, *608*, 499–503. [[CrossRef](#)] [[PubMed](#)]
27. Wang, Y.H.; Steinberg, H.; Jarrillo-Herrero, P.; Gedik, N. Observation of Floquet-Bloch states on the surface of a topological insulator. *Science* **2013**, *342*, 453–457. [[CrossRef](#)] [[PubMed](#)]
28. Carley, R.; Döbrich, K.; Frietsch, B.; Gahl, C.; Teichmann, M.; Schwarzkopf, O.; Wernet, P.; Weinelt, M. Femtosecond Laser Excitation Drives Ferromagnetic Gadolinium out of Magnetic Equilibrium. *Phys. Rev. Lett.* **2012**, *109*, 057401. [[CrossRef](#)] [[PubMed](#)]
29. Eich, S.; Plötzing, M.; Rollinger, M.; Emmerich, S.; Adam, R.; Chen, C.; Kapteyn, H.C.; Murnane, M.M.; Plucinski, L.; Steil, D.; et al. Band structure evolution during the ultrafast ferromagnetic-paramagnetic phase transition in cobalt. *Sci. Adv.* **2017**, *3*, e1602094. [[CrossRef](#)] [[PubMed](#)]
30. Gort, R.; Bühlmann, K.; Däster, S.; Salvatella, G.; Hartmann, N.; Zemp, Y.; Holenstein, S.; Stieger, C.; Fognini, A.; Michlmayr, T.; et al. Early Stages of Ultrafast Spin Dynamics in a $3d$ Ferromagnet. *Phys. Rev. Lett.* **2018**, *121*, 087206. [[CrossRef](#)]
31. Moritz, B.; Kemper, F.; Sentef, M.; Devereaux, T.P.; Freericks, J.K. Electron-Mediated Relaxation Following Ultrafast Pumping of Strongly Correlated Materials: Model Evidence of a Correlation-Tuned Crossover between Thermal and Nonthermal States. *Phys. Rev. Lett.* **2013**, *111*, 077401. [[CrossRef](#)] [[PubMed](#)]
32. Golež, D.; Eckstein, M.; Werner, P. Dynamics of screening in photodoped Mott insulators. *Phys. Rev. B* **2015**, *92*, 195123. [[CrossRef](#)]
33. Wang, Y.; Claassen, M.; Moritz, B.; Devereaux, T.P. Producing coherent excitations in pumped Mott antiferromagnetic insulators. *Phys. Rev. B* **2017**, *96*, 235142. [[CrossRef](#)]
34. Shen, W.; Ge, Y.; Liu, A.Y.; Krishnamurthy, H.R.; Devereaux, T.P.; Freericks, J.K. Nonequilibrium “Melting” of a Charge Density Wave Insulator via an Ultrafast Laser Pulse. *Phys. Rev. Lett.* **2014**, *112*, 176404. [[CrossRef](#)]
35. Hellmann, S.; Rohwer, T.; Kalläne, M.; Hanff, K.; Sohrt, C.; Stange, A.; Carr, A.; Murnane, M.M.; Kapteyn, H.C.; Kipp, L.; et al. Time-domain classification of charge-density-wave insulators. *Nat. Commun.* **2012**, *3*, 1069. [[CrossRef](#)] [[PubMed](#)]
36. Ligges, M.; Avigo, I.; Golež, D.; Strand, H.; Beyazit, Y.; Hanff, K.; Diekmann, F.; Stojchevska, L.; Kalläne, M.; Zhou, P.; et al. Ultrafast Doublon Dynamics in Photoexcited $1T\text{-TaS}_2$. *Phys. Rev. Lett.* **2018**, *120*, 166401. [[CrossRef](#)] [[PubMed](#)]
37. Rohwer, T.; Hellmann, S.; Wiesenmayer, M.; Sohrt, C.; Stange, A.; Slomski, B.; Carr, A.; Liu, Y.; Avila, L.; Kallásiggnne, M.; et al. Collapse of long-range charge order tracked by time-resolved photoemission at high momenta. *Nature* **2011**, *471*, 490–494. [[CrossRef](#)]
38. Burian, M.; Porer, M.; Mardegan, J.R.; Esposito, V.; Parchenko, S.; Burganov, B.; Gurung, N.; Ramakrishnan, M.; Scagnoli, V.; Ueda, H.; et al. Structural involvement in the melting of the charge density wave in $1T\text{-TiSe}_2$. *Phys. Rev. Res.* **2021**, *3*, 13128. [[CrossRef](#)]
39. Dardel, B.; Grioni, M.; Malterre, D.; Weibel, P.; Baer, Y.; Lévy, F. Temperature-dependent pseudogap and electron localization in $1T\text{-TaS}_2$. *Phys. Rev. B* **1992**, *45*, 1462–1465. [[CrossRef](#)]
40. Perfetti, L.; Gloor, T.A.; Mila, F.; Berger, H.; Grioni, M. Unexpected periodicity in the quasi-two-dimensional Mott insulator $1T\text{-TaS}_2$ revealed by angle-resolved photoemission. *Phys. Rev. B* **2005**, *71*, 153101. [[CrossRef](#)]
41. Rosnagel, K.; Smith, N.V. Spin-orbit coupling in the band structure of reconstructed $1T\text{-TaS}_2$. *Phys. Rev. B* **2006**, *73*, 073106. [[CrossRef](#)]
42. Freericks, J.K.; Krishnamurthy, H.R.; Ge, Y.; Liu, A.; Pruschke, T. Theoretical description of time-resolved pump/probe photoemission in TaS_2 : A single-band DFT+DMFT(NRG) study within the quasiequilibrium approximation. *Phys. Status Solidi B* **2009**, *246*, 948–954. [[CrossRef](#)]

43. Rossnagel, K.; Kipp, L.; Skibowski, M. Charge-density-wave phase transition in 1T-TiSe₂: Excitonic insulator versus band-type Jahn-Teller mechanism. *Phys. Rev. B* **2002**, *65*, 235101. [[CrossRef](#)]
44. Kidd, T.; Miller, T.; Chou, M.; Chiang, T.C. Electron-Hole Coupling and the Charge Density Wave Transition in TiSe₂. *Phys. Rev. Lett.* **2002**, *88*, 226402. [[CrossRef](#)] [[PubMed](#)]
45. Cercellier, H.; Monney, C.; Clerc, F.; Battaglia, C.; Despont, L.; Garnier, M.; Beck, H.; Aebi, P.; Patthey, L.; Berger, H.; et al. Evidence for an Excitonic Insulator Phase in 1T-TiSe₂. *Phys. Rev. Lett.* **2007**, *99*, 146403. [[CrossRef](#)] [[PubMed](#)]
46. Rossnagel, K. On the origin of charge-density waves in select layered transition-metal dichalcogenides. *J. Phys. Condens. Matter* **2011**, *23*, 213001. [[CrossRef](#)]
47. Perfetti, L.; Loukakos, P.A.; Lisowski, M.; Bovensiepen, U.; Wolf, M.; Berger, H.; Biermann, S.; Georges, A. Femtosecond dynamics of electronic states in the Mott insulator 1T-TaS₂ by time resolved photoelectron spectroscopy. *New J. Phys.* **2008**, *10*, 053019. [[CrossRef](#)]
48. Fazekas, P.; Tosatti, E. Electrical, structural and magnetic properties of pure and doped 1T-TaS₂. *Philos. Mag. B* **1979**, *39*, 229–244. [[CrossRef](#)]
49. Bayliss, S.C.; Ghorayeb, A.M.; Guy, D.R. Thermal and transport evidence for a phase transition in 1T-TaS₂ observed at 282K upon warming. *J. Phys. C Solid State Phys.* **1984**, *17*. [[CrossRef](#)]
50. Ritschel, T.; Trinckauf, J.; Koepf, K.; Büchner, B.; Zimmermann, M.V.; Berger, H.; Joe, Y.I.; Abbamonte, P.; Geck, J. Orbital textures and charge density waves in transition metal dichalcogenides. *Nat. Phys.* **2015**, *11*, 328–331. [[CrossRef](#)]
51. Petocchi, F.; Nicholson, C.W.; Salzmann, B.; Pasquier, D.; Yazyev, O.V.; Monney, C.; Werner, P. Mott versus Hybridization Gap in the Low-Temperature Phase of 1T-TaS₂. *Phys. Rev. Lett.* **2022**, *129*, 16402. [[CrossRef](#)] [[PubMed](#)]
52. Moritz, B.; Devereaux, T.P.; Freericks, J.K. Time-resolved photoemission of correlated electrons driven out of equilibrium. *Phys. Rev. B* **2010**, *81*, 1–5. [[CrossRef](#)]
53. Wall, S.; Brida, D.; Clark, S.R.; Ehrke, H.P.; Jaksch, D.; Ardavan, A.; Bonora, S.; Uemura, H.; Takahashi, Y.; Hasegawa, T.; et al. Quantum interference between charge excitation paths in a solid-state Mott insulator. *Nat. Phys.* **2011**, *7*, 114–118. [[CrossRef](#)]
54. Di Salvo, F.J.; Moncton, D.E.; Waszczak, J.V. Electronic properties and superlattice formation in the semimetal TiSe₂. *Phys. Rev. B* **1976**, *14*, 4321–4328. [[CrossRef](#)]
55. Woo, K.C.; Brown, F.; McMillan, W.L.; Miller, R.J.; Schaffman, M.J.; Sears, M.P. Superlattice formation in titanium diselenide. *Phys. Rev. B* **1976**, *14*, 3242–3248. [[CrossRef](#)]
56. Monney, G.; Monney, C.; Hildebrand, B.; Aebi, P.; Beck, H. Impact of electron-hole correlations on the 1T-TiSe₂ electronic structure. *Phys. Rev. Lett.* **2015**, *114*, 086402. [[CrossRef](#)]
57. Kogar, A.; Rak, M.S.; Vig, S.; Husain, A.A.; Flicker, F.; Joe, Y.I.; Venema, L.; MacDougall, G.J.; Chiang, T.C.; Fradkin, E.; et al. Signatures of exciton condensation in a transition metal dichalcogenide. *Science* **2017**, *358*, 1314–1317. [[CrossRef](#)] [[PubMed](#)]
58. Van Zandt, L.L.; Honig, J.M. Theories Pertaining to the Semiconductor-Metal Transition in Crystals. *Annu. Rev. Mater. Sci.* **1974**, *4*, 191–220. [[CrossRef](#)]
59. Mathias, S.; Eich, S.; Urbancic, J.; Michael, S.; Carr, A.V.; Emmerich, S.; Stange, A.; Popmintchev, T.; Rohwer, T.; Wiesenmayer, M.; et al. Self-amplified photo-induced gap quenching in a correlated electron material. *Nat. Commun.* **2016**, *7*, 12902. [[CrossRef](#)]
60. Porer, M.; Leierseder, U.; Ménard, J.M.; Dachraoui, H.; Mouchliadis, L.; Perakis, I.E.; Heinzmann, U.; Demsar, J.; Rossnagel, K.; Huber, R. Non-thermal separation of electronic and structural orders in a persisting charge density wave. *Nat. Mater.* **2014**, *13*, 857–861. [[CrossRef](#)]
61. Glover, T.; Schoenlein, R.; Chin, A.; Shank, C. Observation of laser assisted photoelectric effect and femtosecond high order harmonic radiation. *Phys. Rev. Lett.* **1996**, *76*, 2468–2471. [[CrossRef](#)]
62. Bányai, L.; Vu, Q.; Mieck, B.; Haug, H. Ultrafast Quantum Kinetics of Time-Dependent RPA-Screened Coulomb Scattering. *Phys. Rev. Lett.* **1998**, *81*, 882–885. [[CrossRef](#)]
63. Huber, R.; Tauser, F.; Brodschelm, A.; Bichler, M.; Abstreiter, G.; Leitenstorfer, A. How many-particle interactions develop after ultrafast excitation of an electron-hole plasma. *Nature* **2001**, *414*, 286–289. [[CrossRef](#)]
64. Eich, S.; Stange, A.; Carr, A.; Urbancic, J.; Popmintchev, T.; Wiesenmayer, M.; Jansen, K.; Ruffing, A.; Jakobs, S.; Rohwer, T.; et al. Time- and angle-resolved photoemission spectroscopy with optimized high-harmonic pulses using frequency-doubled Ti:Sapphire lasers. *J. Electron Spectrosc. Relat. Phenom.* **2014**, *195*, 231–236. [[CrossRef](#)]
65. Nisoli, M.; De Silvestri, S.; Svelto, O.; Szpöcs, R.; Ferencz, K.; Spielmann, C.; Sartania, S.; Krausz, F. Compression of high-energy laser pulses below 5 fs. *Opt. Lett.* **1997**, *22*, 522–524. [[CrossRef](#)]
66. Rohde, G.; Hendel, A.; Stange, A.; Hanff, K.; Oloff, L.P.; Yang, L.X.; Rossnagel, K.; Bauer, M. Time-resolved ARPES with sub-15 fs temporal and near Fourier-limited spectral resolution. *Rev. Sci. Instrum.* **2016**, *87*, 103102. [[CrossRef](#)]
67. Rohde, G.; Stange, A.; Müller, A.; Behrendt, M.; Oloff, L.P.; Hanff, K.; Albert, T.; Hein, P.; Rossnagel, K.; Bauer, M. Ultrafast Formation of a Fermi-Dirac Distributed Electron Gas. *Phys. Rev. Lett.* **2018**, *121*, 256401. [[CrossRef](#)] [[PubMed](#)]
68. Breusing, M.; Ropers, C.; Elsaesser, T. Ultrafast Carrier Dynamics in Graphite. *Phys. Rev. Lett.* **2009**, *102*, 086809. [[CrossRef](#)] [[PubMed](#)]
69. Malic, E.; Winzer, T.; Bobkin, E.; Knorr, A. Microscopic theory of absorption and ultrafast many-particle kinetics in graphene. *Phys. Rev. B* **2011**, *84*, 205406. [[CrossRef](#)]
70. Malic, E.; Winzer, T.; Knorr, A. Efficient orientational carrier relaxation in optically excited graphene. *Appl. Phys. Lett.* **2012**, *101*, 213110. [[CrossRef](#)]

71. Brida, D.; Tomadin, A.; Manzoni, C.; Kim, Y.J.; Lombardo, A.; Milana, S.; Nair, R.R.; Novoselov, K.S.; Ferrari, A.C.; Cerullo, G.; et al. Ultrafast collinear scattering and carrier multiplication in graphene. *Nat. Commun.* **2013**, *4*, 2987. [[CrossRef](#)] [[PubMed](#)]
72. Jager, M.F.; Ott, C.; Kraus, P.M.; Kaplan, C.J.; Pouse, W.; Marvel, R.E.; Haglund, R.F.; Neumark, D.M.; Leone, S.R. Tracking the insulator-to-metal phase transition in VO₂ with few-femtosecond extreme UV transient absorption spectroscopy. *Proc. Natl. Acad. Sci. USA* **2017**, *114*, 9558–9563. [[CrossRef](#)] [[PubMed](#)]
73. Chang, H.T.; Guggenmos, A.; Chen, C.T.; Oh, J.; Géneaux, R.; Chuang, Y.D.; Schwartzberg, A.M.; Aloni, S.; Neumark, D.M.; Leone, S.R. Coupled valence carrier and core-exciton dynamics in WS₂ probed by few-femtosecond extreme ultraviolet transient absorption spectroscopy. *Phys. Rev. B* **2021**, *104*, 064309. [[CrossRef](#)]
74. Sidiropoulos, T.P.; Di Palo, N.; Rivas, D.E.; Severino, S.; Reduzzi, M.; Nandy, B.; Bauerhenne, B.; Krylow, S.; Vasileiadis, T.; Danz, T.; et al. Probing the Energy Conversion Pathways between Light, Carriers, and Lattice in Real Time with Attosecond Core-Level Spectroscopy. *Phys. Rev. X* **2021**, *11*, 41060. [[CrossRef](#)]
75. Geneaux, R.; Marroux, H.J.; Guggenmos, A.; Neumark, D.M.; Leone, S.R. Transient absorption spectroscopy using high harmonic generation: A review of ultrafast X-ray dynamics in molecules and solids. *Philos. Trans. R. Soc. A* **2019**, *377*. [[CrossRef](#)] [[PubMed](#)]
76. Cavalieri, A.L.; Müller, N.; Uphues, T.; Yakovlev, V.S.; Baltuska, A.; Horvath, B.; Schmidt, B.; Blümel, L.; Holzwarth, R.; Hendel, S.; et al. Attosecond spectroscopy in condensed matter. *Nature* **2007**, *449*, 1029–1032. [[CrossRef](#)]
77. Neppel, S.; Ernstorfer, R.; Cavalieri, A.L.; Lemell, C.; Wachter, G.; Magerl, E.; Bothschafter, E.M.; Jobst, M.; Hofstetter, M.; Kleineberg, U.; et al. Direct observation of electron propagation and dielectric screening on the atomic length scale. *Nature* **2015**, *517*, 342–346. [[CrossRef](#)] [[PubMed](#)]
78. Siek, F.; Neb, S.; Bartz, P.; Hensen, M.; Strüber, C.; Fiechter, S.; Torrent-Sucarrat, M.; Silkin, V.M.; Krasovskii, E.E.; Kabachnik, N.M.; et al. Angular momentum-induced delays in solid-state photoemission enhanced by intra-atomic interactions. *Science* **2017**, *357*, 1274–1277. [[CrossRef](#)] [[PubMed](#)]
79. Locher, R.; Castiglioni, L.; Lucchini, M.; Greif, M.; Gallmann, L.; Osterwalder, J.; Hengsberger, M.; Keller, U. Energy-dependent photoemission delays from noble metal surfaces by attosecond interferometry. *Optica* **2015**, *2*, 405–410. [[CrossRef](#)]
80. Tao, Z.; Chen, C.; Szilvási, T.; Keller, M.; Mavrikakis, M.; Kapteyn, H.; Murnane, M. Direct time-domain observation of attosecond final-state lifetimes in photoemission from solids. *Science* **2016**, *353*, aaf6793. [[CrossRef](#)]
81. Krausz, F.; Stockman, M.I. Attosecond metrology: From electron capture to future signal processing. *Nat. Photonics* **2014**, *8*, 205–213. [[CrossRef](#)]
82. Kruchinin, S.Y.; Krausz, F.; Yakovlev, V.S. Colloquium: Strong-field phenomena in periodic systems. *Rev. Mod. Phys.* **2018**, *90*, 21002. [[CrossRef](#)]
83. Higuchi, T.; Heide, C.; Ullmann, K.; Weber, H.B.; Hommelhoff, P. Light-field-driven currents in graphene. *Nature* **2017**, *550*, 224–228. [[CrossRef](#)] [[PubMed](#)]
84. Heide, C.; Higuchi, T.; Weber, H.B.; Hommelhoff, P. Coherent Electron Trajectory Control in Graphene. *Phys. Rev. Lett.* **2018**, *121*, 207401. [[CrossRef](#)]
85. Breusing, M.; Kuehn, S.; Winzer, T.; Malić, E.; Milde, F.; Severin, N.; Rabe, J.; Ropers, C.; Knorr, A.; Elsaesser, T. Ultrafast nonequilibrium carrier dynamics in a single graphene layer. *Phys. Rev. B* **2011**, *83*, 153410. [[CrossRef](#)]
86. Oloff, L.P.; Hanff, K.; Stange, A.; Rohde, G.; Diekmann, F.; Bauer, M.; Rossnagel, K. Pump laser-induced space-charge effects in HHG-driven time- and angle-resolved photoelectron spectroscopy. *J. Appl. Phys.* **2016**, *119*, 225106. [[CrossRef](#)]
87. Kuzmenko, A.B.; Van Heumen, E.; Carbone, F.; Van Der Marel, D. Universal optical conductance of graphite. *Phys. Rev. Lett.* **2008**, *100*, 2–5. [[CrossRef](#)] [[PubMed](#)]
88. Papoular, R.J.; Papoular, R. Some optical properties of graphite from IR to millimetric wavelengths. *Mon. Not. R. Astron. Soc.* **2014**, *443*, 2974–2982. [[CrossRef](#)]
89. Kelardeh, H.K.; Apalkov, V.; Stockman, M.I. Attosecond strong-field interferometry in graphene: Chirality, singularity, and Berry phase. *Phys. Rev. B* **2016**, *93*, 155434. [[CrossRef](#)]
90. Aeschlimann, M.; Brixner, T.; Fischer, A.; Kramer, C.; Melchior, P.; Pfeiffer, W.; Schneider, C.; Strüber, C.; Tuchscherer, P.; Voronine, D.V. Coherent Two-Dimensional Nanoscopy. *Science* **2011**, *333*, 1723–1726. [[CrossRef](#)]
91. Reutz, M.; Li, A.; Wang, Z.; Petek, H. Coherent multidimensional photoelectron spectroscopy of ultrafast quasiparticle dressing by light. *Nat. Commun.* **2020**, *11*, 2230. [[CrossRef](#)] [[PubMed](#)]
92. Uhl, D.; Bangert, U.; Bruder, L.; Stienkemeier, F. Coherent optical 2D photoelectron spectroscopy. *Optica* **2021**, *8*, 1316–1324. [[CrossRef](#)]
93. Ogawa, S.; Nagano, H.; Petek, H.; Heberle, A.P. Optical Dephasing in Cu(111) Measured by Interferometric Two-Photon Time-Resolved Photoemission. *Phys. Rev. Lett.* **1997**, *78*, 1339–1342. [[CrossRef](#)]
94. Petek, H.; Nagano, H.; Ogawa, S. Hole decoherence of d bands in copper. *Phys. Rev. Lett.* **1999**, *83*, 832–835. [[CrossRef](#)]
95. Cui, X.; Wang, C.; Argondizzo, A.; Garrett-Roe, S.; Gumhalter, B.; Petek, H. Transient excitons at metal surfaces. *Nat. Phys.* **2014**, *10*, 505–509. [[CrossRef](#)]
96. Randi, F.; Fausti, D.; Eckstein, M. Bypassing the energy-time uncertainty in time-resolved photoemission. *Phys. Rev. B* **2017**, *95*, 115132. [[CrossRef](#)]
97. Mukamel, S. *Principles of Nonlinear Optics and Spectroscopy*; Oxford University Press: Oxford, UK, 1995.
98. Mukamel, S. Multidimensional femtosecond correlation spectroscopies of electronic and vibrational excitations. *Annu. Rev. Phys. Chem.* **2000**, *51*, 691–729. [[CrossRef](#)] [[PubMed](#)]

99. Buss, J.H.; Wang, H.; Xu, Y.; Maklar, J.; Joucken, F.; Zeng, L.; Stoll, S.; Jozwiak, C.; Pepper, J.; Chuang, Y.D.; et al. A setup for extreme-ultraviolet ultrafast angle-resolved photoelectron spectroscopy at 50-kHz repetition rate. *Rev. Sci. Instrum.* **2018**, *90*, 023105. [[CrossRef](#)] [[PubMed](#)]
100. Puppin, M.; Deng, Y.; Nicholson, C.W.; Feldl, J.; Schroeter, N.; Vita, H.; Kirchmann, P.S.; Monney, C.; Rettig, L.; Wolf, M.; et al. Time- and angle-resolved photoemission spectroscopy of solids in the extreme ultraviolet at 500 kHz repetition rate. *Rev. Sci. Instrum.* **2018**, *90*, 023104. [[CrossRef](#)]
101. Mills, A.K.; Zhdanovich, S.; Na, M.X.; Boschini, F.; Razzoli, E.; Michiardi, M.; Sheyerman, A.; Schneider, M.; Hammond, T.J.; Süß, V.; et al. Cavity-enhanced high harmonic generation for extreme ultraviolet time- and angle-resolved photoemission spectroscopy. *Rev. Sci. Instrum.* **2019**, *90*, 083001. [[CrossRef](#)]
102. Chini, M.; Mashiko, H.; Wang, H.; Chen, S.; Yun, C.; Scott, S.; Gilbertson, S.; Chang, Z. Delay control in attosecond pump-probe experiments. *Opt. Express* **2009**, *17*, 21459–21464. [[CrossRef](#)] [[PubMed](#)]

Disclaimer/Publisher's Note: The statements, opinions and data contained in all publications are solely those of the individual author(s) and contributor(s) and not of MDPI and/or the editor(s). MDPI and/or the editor(s) disclaim responsibility for any injury to people or property resulting from any ideas, methods, instructions or products referred to in the content.